RSC Advances

PAPER

View Article Online
View Journal | View Issue

Cite this: *RSC Adv.*, 2020, **10**, 18124

Calculation of magnetic response properties of tetrazines†

Mesías Orozco-Ic, [a] Christian A. Celaya [ab] and Dage Sundholm *[a]

Magnetic response properties of 1,2,3,5-tetrazine derivatives including the newly synthesized 4,6-diphenyl-1,2,3,5-tetrazine have been studied computationally at the density functional theory (DFT) level. Calculations of magnetically induced current densities and induced magnetic fields show that the unsubstituted 1,2,3,5-tetrazine is almost as aromatic as benzene. Separating the magnetic shielding functions into molecular orbital components provided additional insights into the magnetic response. The aromatic character estimated from magnetically induced current densities and induced magnetic fields shows that $NICS^{\pi}_{zz}(0)$ values and ring-current strengths yield about the same degree of aromaticity, whereas $NICS_{zz}(0)$ and $NICS_{zz}(1)$ values are contaminated by σ electron contributions. The studied 1,2,3,5-tetrazine derivatives are less aromatic than the unsubstituted one. Calculations of magnetic response properties of 4,6-diphenyl-1,2,3,5-tetrazine showed that it is the least aromatic among the studied molecules according to the ring-current criterion, while 4,6-[1,2,3,5]-ditetrazinyl-1,2,3,5-tetrazine is as aromatic as 4,6-dimethyl-1,2,3,5-tetrazine and slightly less aromatic than the unsubstituted 1,2,3,5-tetrazine.

Received 20th February 2020
Accepted 1st May 2020

DOI: 10.1039/d0ra01641a

rsc.li/rsc-advances

Introduction

Novel methods for synthesizing heterocyclic aromatic molecules such as di-, tri- and tetrazines have recently been developed.[1–8] 1,3-Diazine (pyrimidine) is one of the more important azines, because its derivatives are of biological relevance as building blocks in the nucleobases of deoxyribonucleic acid (DNA).[9,10] Triazines have been widely studied because of their use in biological and industrial applications.[11–13] The molecular structures of the three possible tetrazine isomers (1,2,3,4-tetrazine, 1,2,3,5-tetrazine, and 1,2,4,5-tetrazine) differ by the relative positions of the nitrogen atoms in the six-membered ring,[13–15] of which 1,2,4,5-tetrazine is the easiest one to synthesize, because it has only two nitrogens next to each other. Tetrazine derivatives are recognized as high-energy density materials (HEDMs) due to their high nitrogen content, strong N–N and N–C bonds, large heat of formation, high thermal stability and suitable structural properties.[15–22] The aromatic properties of tetrazine have been previously studied by Wang *et al.*,[23] who based on nucleus independent chemical shift (NICS)[24,25] calculations and by using energy criteria concluded that the aromatic character is about the same for all azines they studied. In their NICS(0) studies, they found that the three tetrazine isomers are non-aromatic, while $NICS^{\pi}_{zz}(0)$ calculations suggested that 1,2,3,5-tetrazine is the least aromatic among the three isomers.[23] Yang *et al.* found that the NICS(0) value decreases with increasing number of nitrogens in the ring suggesting that tetrazines are less aromatic than triazines and so on.[26] Sanchez-Sanz obtained the similar trend for the NICS(0) values of the azines, whereas the NICS(1) and NICS(2) values were found to be almost independent of the number of nitrogens in the ring.[27] Wu and Boger recently synthesized 4,6-diphenyl-1,2,3,5-tetrazine and found that is aromatic.[8]

In this work, we investigate the aromatic properties of tetrazines by calculating magnetically induced current densities and induced magnetic fields of unsubstituted and substituted

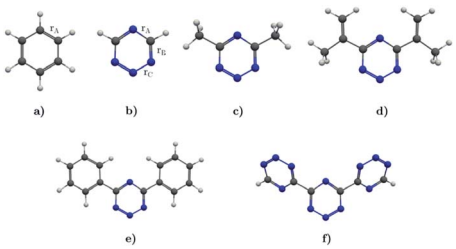

Fig. 1 The molecular structure of (a) benzene, (b) 1,2,3,5-tetrazine, (c) 4,6-dimethyl-1,2,3,5-tetrazine, (d) 4,6-bis(1-methylethenyl)-1,2,3,5-tetrazine, (e) 4,6-diphenyl-1,2,3,5-tetrazine, and (f) 4,6-[1,2,3,5]-ditetrazinyl-1,2,3,5-tetrazine.

[a]*Department of Chemistry, University of Helsinki, P. O. Box 55, A. I. Virtasen aukio 1, FIN-00014 Helsinki, Finland. E-mail: dage.sundholm@helsinki.fi*

[b]*Departamento de Materiales de Baja Dimensionalidad, Instituto de Investigaciones en Materiales, Universidad Nacional Autónoma de México, Apartado Postal 70-360, Ciudad de México 04510, Mexico*

† Electronic supplementary information (ESI) available: Tables S1–S3, Fig. S1–S7 and Cartesian coordinates of the molecular structures. See DOI: 10.1039/d0ra01641a

1,2,3,5-tetrazines. The calculations yield qualitative and quantitative information about electron delocalization and the degree of aromaticity of the tetrazine ring.[28–33] The studied molecules comprise 1,2,3,5-tetrazine, 4,6-dimethyl-1,2,3,5-tetrazine, 4,6-bis(1-methylethenyl)-1,2,3,5-tetrazine, 4,6-diphenyl-1,2,3,5-tetrazine, and 4,6-[1,2,3,5]-ditetrazinyl-1,2,3,5-tetrazine, which are shown in Fig. 1. Magnetic response properties of the two others unsubstituted tetrazine isomers are given as ESI.†

Computational details

The molecular structures were fully optimized at the density functional theory (DFT) level using the PBE0 hybrid functional and triple-zeta valence basis set augmented with polarization functions (def2-TZVP).[34–36] Grimme's semi-empirical dispersion correction (D3) was used for considering van der Waals interactions.[37] Bond lengths and HOMO–LUMO gaps are given in Table S1 of the ESI.† External magnetic fields induce current densities (J^{ind}) in molecules, which gives rise to a secondary induced magnetic field (B^{ind})[28–33,38–42] that is proportional to the magnetic shielding tensor.[42] In aromatic ring-shaped molecules, the magnetic response is diamagnetic, *i.e.*, a net diatropic ring current is sustained by the aromatic ring, whereas antiaromatic rings sustain a net paratropic ring current.[28–33] Nuclear magnetic resonance (NMR) shielding and current-density calculations were performed at the PBE0 level using split-valence basis sets augmented with polarization functions (def2-SVP).[43] Gauge-including atomic orbitals (GIAOs) were used in the NMR shielding and current-density calculations.[44,45] The electronic structure calculations were performed with the Gaussian 16 software.[46] Current densities were calculated using the gauge-including magnetically induced current (GIMIC) method,[28–30] which is freely available and interfaced to Gaussian 16.[47] The current densities are visualized with ParaView.[48] The B^{ind} was calculated using the Aromagnetic code,[49] which is also interfaced to Gaussian 16 and visualized with VisIt.[50] The external magnetic field was aligned along the highest symmetry axis of the molecular ring. Thus, the z component of the induced magnetic field (B_z^{ind}) is the most important one providing information about the aromatic character of the molecular ring.[31–33] B_z^{ind} (in ppm) is numerically equivalent to $NICS_{zz}$ values.[31–33] The calculated B^{ind} was separated into its molecular orbitals (MOs) contributions[32,51] using the NBO6 code[52] *via* the Natural Chemical Shielding (NCS) analysis.[53] Ring-current strength susceptibilities, (J^{ind} in nA T^{-1}) were obtained with the GIMIC program by performing numerical integration of the current density flowing through a plane from the center of the ring to a very far distance outside the ring, where the current density vanishes.[28–30] The height of the plane is 8 bohr above and below the ring plane. Ring-current strength susceptibilities are called ring-current strengths in the rest of the paper. The same ring-current strength is obtained for all bonds of the ring, when the basis-set is complete.[28] Ring-current strengths reported for different bonds in Table S2 of the ESI† show very small discrepancies, even though the rather small SVP basis set was used. The lower symmetry of the tetrazine ring as compared to benzene may lead to nonvertical current-density vortices that also affect the accuracy of the numerical integration, because some ring-current strength contributions may fall outside the integration plane.

Results and discussion

Benzene and 1,2,3,5-tetrazine

Benzene is the archetypal aromatic molecule with 6π electrons fulfills Hückel's rule for aromaticity.[54,55] The molecular structure belongs to the D_{6h} point group. The length of the conjugated bonds is 1.39 Å and it has a large HOMO–LUMO gap of 7.11 eV at the PBE0 level, so, this is a very stable molecule. An external magnetic field perpendicular to the molecular ring induces a diatropic ring current in aromatic molecules, which is visualized as the clockwise direction in Fig. 2.[38–41] A weaker paratropic (counterclockwise) ring current involving mainly the σ orbitals flows in the molecular plane inside the ring.[56–58] It has been shown that at a distance of 1 bohr from the molecular plane the π electrons dominates in ring current density.[58–60] Numerical integration yields a net diatropic ring-current strength (J^{ind}) of 12.05 nA T^{-1}. The J^{ind} of the studied molecules are summarized in Table 1. The ring current of benzene induces a secondary field (B^{ind}) in the opposite direction to the applied one, which leads to negative B_z^{ind} values.[31–33] The MO partitions of the shielding tensor obtained with the NCS-GIAO method[53] lead to large core contributions, which have been found to increase with the number of atoms in the ring.[61] Core contributions to the magnetic shielding determined from orbital current densities that are calculated using the ipsocentric approach[60,62] are much smaller, because it avoids rotations of occupied orbitals that cause gauge-origin problems.[60,62–64] The two approaches yield the same shielding contributions from σ and π orbitals of planar molecules that cannot mix through orbital rotations.[60,62] Therefore, we do not calculate orbital contributions from individual orbitals but divide the magnetic shieldings into contributions from σ (core + σ) and π orbitals. B_z^{ind} has shielding cones (shown in blue) above and below the ring, while the σ electrons are responsible for the positive deshielding regions (shown in red) outside the ring as

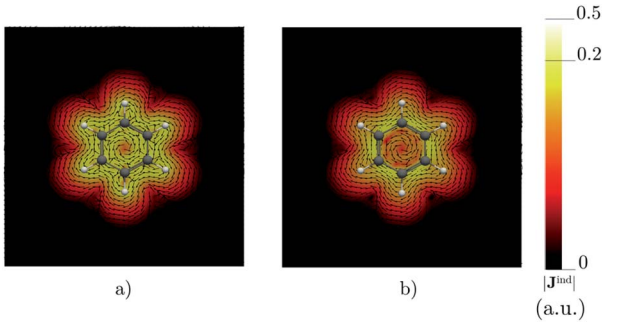

Fig. 2 The current density (J^{ind}) plotted at (a) 0 bohr and (b) 1 bohr from the molecular plane of benzene. $|J^{ind}|$ values are given in atomic units (1 a.u. = 100.63 nA T^{-1} $Å^{-2}$). The figure was made with ParaView.[48]

Table 1 Integrated strengths (in nA T^{-1}) of the diatropic, paratropic and net ring current of the studied molecules. The current densities were calculated at the PBE0/def2-SVP level

Molecule	Core + σ	π	Total
Benzene	23.21	−36.41	−13.20
1,2,3,5-Tetrazine	29.58	−35.94	−6.36
4,6-Dimethyl-1,2,3,5-tetrazine	27.88	−31.15	−3.27
4,6-Bis(1-methylethenyl)-1,2,3,5-tetrazine	29.42	−26.30	3.12
4,6-Diphenyl-1,2,3,5-tetrazine	30.31	−20.65	9.66
4,6-[1,2,3,5]-Ditetrazinyl-1,2,3,5-tetrazine	22.17	−26.83	−4.66

Table 2 Orbital contributions to the B_z^{ind} values (in ppm) computed in the center of the studied molecules ($NICS_{zz}(0)$) calculated at the PBE0/def2-SVP level

Molecule	Diatropic	Paratropic	Net
Benzene	17.32	−5.27	12.05
1,2,3,5-Tetrazine	15.39	−5.31	10.08
4,6-Dimethyl-1,2,3,5-tetrazine	14.82	−5.50	9.32
4,6-Bis(1-methylethenyl)-1,2,3,5-tetrazine	13.87	−5.84	8.03
4,6-Diphenyl-1,2,3,5-tetrazine	12.81	−6.14	6.66
4,6-[1,2,3,5]-Ditetrazinyl-1,2,3,5-tetrazine	14.64	−5.17	9.46

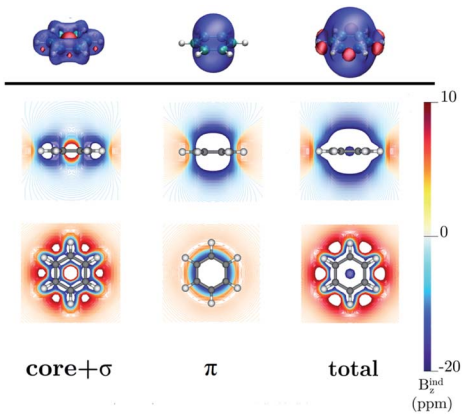

Fig. 3 The isosurfaces of the B_z^{ind} of benzene are shown in the upper panel. The shielding and deshielding cones at −10 ppm and 10 ppm are in blue and red, respectively. The B_z^{ind} isolines calculated in the transverse and molecular planes are shown in the lower panel. The figure was made with VisIt.[50]

shown in Fig. 3.[31–33,51] The B_z^{ind} calculated along the symmetry axis (z axis) shown in Fig. 4 also provides qualitative and quantitative information about the degree of aromaticity.[25,65–67] The total B_z^{ind} declines asymptotically as z^{-3} for large z.[65] The π contribution ($B_{z,\pi}^{ind}$), which has a similar mathematical shape at large distances,[68,69] has a minimum of −36.41 ppm in the center of the ring and large negative values along the z axis. These are about −13 ppm even at 2 Å from the ring center. Orbital contributions to the negative B_z^{ind} values calculated in the ring center ($NICS_{zz}(0)$ values)[24,25] are given in Table 2. The core + σ contribution is 23.21 ppm at the ring center representing the maximum value of the profile. It almost cancels the π contribution near the ring, but it declines rapidly with increasing z.[63,64,66,67] Although the maximum and minimum values vary from one system to another, the magnetic behavior is largely the same for the studied molecules. Thus, the $NICS_{zz}(0)$, $NICS_{zz}(1)$ and even the $NICS_{zz}(2)$ indexes are contaminated with core + σ contributions affecting the estimated degree of aromaticity in the systems from $NICS_{zz}$ values. The $B_{z,\pi}^{ind}(0)$ value, which is equivalent to the $NICS_{zz}^{\pi}(0)$, is therefore a better aromaticity index for the studied molecules.

Calculations on 1,2,3,5-tetrazine, whose molecular structure belongs to the C_{2v} point group with 6π electrons is expected to be aromatic according to the Hückel rule. The addition of the functional groups to the 1,2,3,5-tetrazine ring does not significantly affect the HOMO–LUMO gap (see Table S1†). The average HOMO–LUMO gap of 4.52 eV of the studied 1,2,3,5-tetrazines is much smaller than for benzene. However, the 1,2,3,5-tetrazine has a HOMO–LUMO gap of 4.85 eV, which is much smaller than for benzene. The current-density plot in Fig. 5 shows that 1,2,3,5-tetrazine sustains a diatropic ring current above, below and outside the ring, whereas it sustains a paratropic ring current inside the ring as benzene. The integrated ring-current strengths in Table 1 show that 1,2,3,5-tetrazine sustains a net ring current of 10.08 nA T^{-1}, which is only 2 nA T^{-1} weaker than

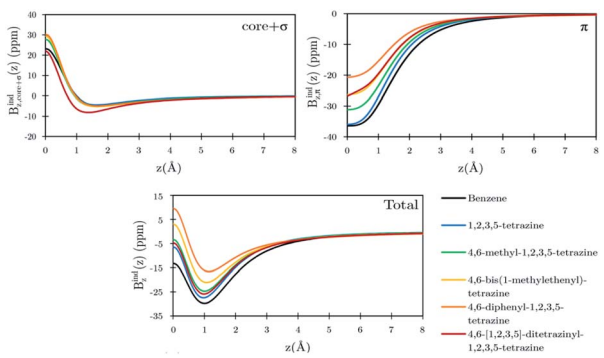

Fig. 4 Orbital contributions to the B_z^{ind} profiles along the z-axis for benzene and the tetrazines calculated at the PBE0/def2-SVP level. The z axis of the profile calculation passes through the center of the benzene/tetrazine ring.

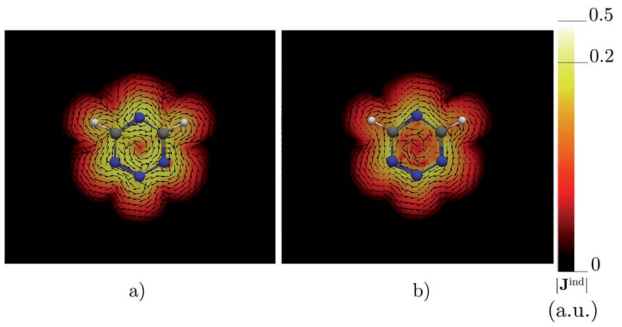

Fig. 5 The current density (J^{ind}) plotted at (a) 0 bohr and (b) 1 bohr from the molecular plane of 1,2,3,5-tetrazine. $|J^{ind}|$ values are given in atomic units (1 a.u. = 100.63 nA T^{-1} $Å^{-2}$). The figure was made with ParaView.[48]

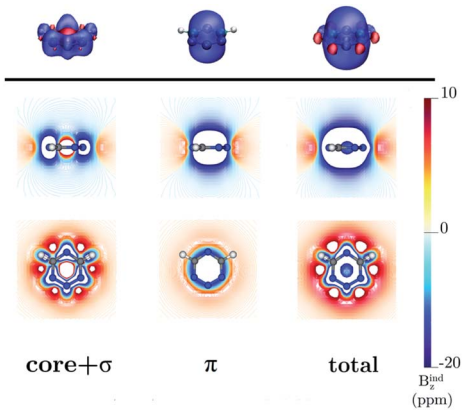

Fig. 6 The isosurfaces of the B_z^{ind} of 1,2,3,5-tetrazine are shown in the upper panel. The shielding and deshielding cones at −10 ppm and 10 ppm are in blue and red, respectively. The B_z^{ind} isolines calculated in the transverse and molecular planes are shown in the lower panel. The figure was made with VisIt.[50]

for benzene. The calculated $B_{z,\pi}^{ind}(0)$ value of −35.94 ppm also suggest that 1,2,3,5-tetrazine is almost as aromatic as benzene. The orbital contributions to B_z^{ind} shown in profiles and plots of Fig. 4 and 6, respectively, look qualitatively like those obtained for benzene. The π contribution to the magnetic shielding of the tetrazines are practically the same as for benzene, whereas the core + σ contribution is about 7 ppm larger in the ring center than for benzene. Thus, according to the magnetic criteria 1,2,3,5-tetrazine is less aromatic than benzene. The two other tetrazine isomers (1,2,3,4-tetrazine and 1,2,4,5-tetrazine) have a similar magnetic response as 1,2,3,5-tetrazine. Their ring-current strengths and $B_z^{ind}(0)$ values are reported in Tables S2 and S3 of the ESI.† The magnetic response properties of 1,2,3,4-tetrazine and 1,2,4,5-tetrazine are not discussed further in this work.

4,6-Dimethyl- and 4,6-bis(1-methylethenyl)-1,2,3,5-tetrazine

We studied 4,6-dimethyl-1,2,3,5-tetrazine and 4,6-bis(1-methylethenyl)-1,2,3,5-tetrazine in order to understand how alkyl substituents affect the aromatic character of the tetrazine ring. The geometry and HOMO–LUMO gap of the tetrazine ring are not significantly affected by the methyl or methylethenyl substitution. The calculated ring-current strengths show that 4,6-dimethyl-1,2,3,5-tetrazine and 4,6-bis(1-methylethenyl)-1,2,3,5-tetrazine are aromatic sustaining ring currents of 9.32 nA T^{-1} and 8.03 nA T^{-1}, respectively. Thus, the alkyl substitution leads to 1–2 nA T^{-1} weaker ring currents. A current strength of 6.93 nA T^{-1} flows along the C–C bond between the methyl substituents and the tetrazine ring, whereas only 2.4 nA T^{-1} continues along the ring. The corresponding current strengths for 4,6-bis(1-methylethenyl)-1,2,3,5-tetrazine are 6.41 nA T^{-1} and 1.6 nA T^{-1} for the outer and inner pathway, respectively. The current densities of 4,6-dimethyl-1,2,3,5-tetrazine and 4,6-bis(1-methylethenyl)-1,2,3,5-tetrazine are given in Fig. S1 and S3 of the ESI† and the orbital contributions to B_z^{ind} are shown in Fig. S2 and S4 of the ESI.† The ring-current pathway is on the outside of the alkyl substituents as shown in the streamline representation of J^{ind} in Fig. S5 of the ESI.† Calculations of the magnetic response show that the alkyl substituted tetrazines are aromatic but slightly less than the unsubstituted tetrazine ring.

4,6-Diphenyl- and 4,6-[1,2,3,5]-ditetrazinyl-1,2,3,5-tetrazine

The ring-current strength of 4,6-diphenyl-1,2,3,5-tetrazine is 6.66 nA T^{-1}, which is 3.42 nA T^{-1} weaker than the ring-current for the unsubstituted tetrazine. NMR signals were detected.[8] Calculations yielded a rotational barrier of 31 kJ mol^{-1} implying that the phenyl groups rotate at room temperature. The interaction between the phenyl hydrogens in the *ortho* position and the nitrogens of the tetrazine ring as well as the common ring current stabilize the planar structure. The pictures of the current density maps and streamlines in Fig. 7 and 8 show a global ring current around the three rings. Calculations of the B^{ind} also suggest that the phenyl-substituted is the least aromatic of the studied molecules because the shielding cone of the tetrazine ring is smaller than for the unsubstituted ring (Fig. 9). This can also be seen in the $B_{z,\pi}^{ind}$ profile (Fig. 4), because for this system the minimum is the least pronounced. The $B_{z,\pi}^{ind}(0)$ value of −20.65 ppm is in absolute value about 15 ppm smaller than for the unsubstituted tetrazine ring, which correlates well with the calculated ring-current strengths. The trend of the $B_{z,\pi}^{ind}(0)$ values of the studied tetrazines is largely the same as the one obtained for the ring-current strengths. On the other hand, the central ring of 4,6-[1,2,3,5]-ditetrazinyl-1,2,3,5-tetrazine is planar, whereas the tetrazine substituents are slightly tilted with respect to the ring in the middle. The strength of the ring current that flows along the C–C bond between two tetrazine rings is 4.81 nA T^{-1}, which is half the total ring-current strength of 9.46 nA T^{-1} for the tetrazine ring in the middle. Thus, the ring current splits into local and global pathways at the tetrazine substituents as shown in Fig. 7. The current density in Fig. S6 of the ESI† shows that 4,6-[1,2,3,5]-ditetrazinyl-1,2,3,5-tetrazine sustains a similar diatropic ring current in the central ring of tetrazine as dimethyl-substituted tetrazine, which have almost the same $B_{z,\pi}^{ind}(0)$ values, as seen in Table 2. The $B_{z,\pi}^{ind}(0)$ value for 4,6-[1,2,3,5]-ditetrazinyl-1,2,3,5-tetrazine of −26.83 ppm is in absolute value 4.32 ppm smaller than for the unsubstituted tetrazine showing that the degree of aromaticity is in qualitative agreement with the one deduced

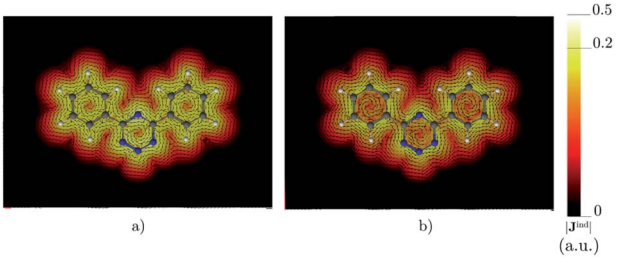

Fig. 7 The current density (J^{ind}) plotted at (a) 0 bohr and (b) 1 bohr from the molecular plane of 4,6-diphenyl-1,2,3,5-tetrazine. $|J^{ind}|$ values are given in atomic units (1 a.u. = 100.63 nA T^{-1} $Å^{-2}$). The figure was made with ParaView.[48]

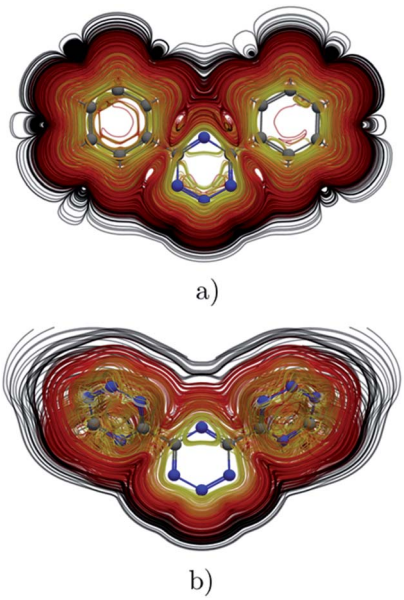

Fig. 8 Streamlines representation of J^{ind} for (a) 4,6-diphenyl-1,2,3,5-tetrazine showing the global ring current pathways, and the local and global ones for (b) 4,6-[1,2,3,5]-ditetrazinyl-1,2,3,5-tetrazine. The figure was made with ParaView.[48]

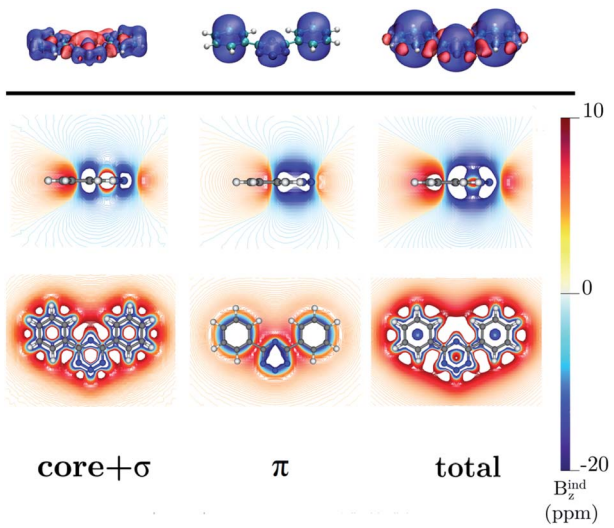

Fig. 9 The isosurfaces of the B_z^{ind} of 4,6-diphenyl-1,2,3,5-tetrazine are shown in the upper panel. The shielding and deshielding cones at −10 ppm and 10 ppm are in blue and red, respectively. The B_z^{ind} plots calculated in the transverse and molecular planes are shown in the lower panel. The figure was made with VisIt.[50]

from ring-current strengths. The same can be concluded from the B_z^{ind} plots in Fig. S7 of the ESI.†

Conclusions

Calculations of magnetically induced current densities and induced magnetic fields show that unsubstituted 1,2,3,5-tetrazine is aromatic sustaining a net diatropic ring current when it is exposed to an external magnetic field perpendicular to the ring. The behavior of the magnetic responses is like that of benzene. The calculations show that there is a correlation between ring-current strengths and $B_{z,\pi}^{ind}(0)$ values, whereas $NICS_{zz}(0)$, $NICS_{zz}(1)$ and $NICS_{zz}(2)$ values are contaminated by core and σ contributions leading to uncertainties in the degree of aromaticity based on them. Calculations of the magnetic response of the substituted 1,2,3,5-tetrazines shows that the substituents are an integrated part of the aromatic system. In the case of 4,6-diphenyl-1,2,3,5-tetrazine, the tetrazine ring does not only sustains a ring current of its own but there is also a global ring current flowing along the C–C single bond between the tetrazine and phenyl rings and continues outside of the phenyl rings. The global aromaticity and the interaction between the hydrogens in the *ortho* position of the phenyls and the nitrogens of the tetrazine ring stabilize 4,6-diphenyl-1,2,3,5-tetrazine. Calculations of the aromatic character of 4,6-[1,2,3,5]-ditetrazinyl-1,2,3,5-tetrazine showed that it has an aromatic tetrazine ring in the middle. The calculations also showed that a global ring-current flows around the three tetrazine rings. The ring current splits almost equally into a local ring current around the tetrazine ring in the middle and the global ring current.

Conflicts of interest

There are no conflicts to declare.

Acknowledgements

This research has been supported by the Academy of Finland through project 314821. CSC – the Finnish IT Center for Science and the Finnish Grid and Cloud Infrastructure (persistent identifier urn:nbn:fi:research-infras-2016072533) are acknowledged for computer time. We thank Magnus Ehrnrooth foundation and the Swedish Cultural Foundation in Finland for financial support. M. O.-I. and C. A. C. also thank Conacyt for their PhD fellowships. The authors thank the anonymous reviewers who helped to improve our article with important suggestions.

References

1 M. H. V. Huynh, M. A. Hiskey, D. E. Chavez, D. L. Naud and R. D. Gilardi, *J. Am. Chem. Soc.*, 2005, **127**, 12537–12543.
2 M. Savastano, C. García-Gallarín, M. D. L. de la Torre, C. Bazzicalupi, A. Bianchi and M. Melguizo, *Coord. Chem. Rev.*, 2019, **397**, 112–137.
3 A. P. Brucks, 1,2,4,5-Tetrazine, *Encycl. Reagents Org. Synth.*, 2015, 1–2.
4 H. M. M. Dalloul, *Heterocycl. Commun.*, 2003, **9**, 307–312.
5 X.-F. Wu and Z. Wang, Synthesis of Triazine. Transition Metal Catalyzed Pyrimidine, Pyrazine, Pyridazine and Triazine Synthesis, *Synthesis of Triazine*, 2017, ch. 5, pp. 79–93.
6 X.-F. Wu and Z. Wang, Synthesis of Triazine. Transition Metal Catalyzed Pyrimidine, Pyrazine, Pyridazine and

Triazine Synthesis, *Synthesis of Triazine*, 2017, ch. 4, pp. 73–77.
7 A. A. Konnov, M. S. Klenov, A. M. Churakov, Y. A. Strelenko, A. O. Dmitrienko, L. N. Puntus, K. A. Lyssenko and V. A. Tartakovsky, *Asian J. Org. Chem.*, 2018, **7**, 2534–2543.
8 Z.-C. Wu and D. L. Boger, *J. Am. Chem. Soc.*, 2019, **141**, 16388–16397.
9 A. R. Aroor, *Chemistry of Nucleic Acids. Medical Biochemistry*, 2011, ch. 8, pp. 543–555.
10 E. Rosenberg, Chemistry of DNA, *It's in Your DNA*, 2017, ch. 2, pp. 9–16.
11 R. Patel and A. Malhotra, *Triazines: Synthesis, Applications, and Toxicity*, Nova Science Pub Incorporated, 1st edn, 2012, pp. 1–209.
12 O. Bekircan, M. Küxük, B. Kahveci and S. Kolayli, *Arch. Pharm.*, 2005, **338**, 365–372.
13 H. Neunhoeffer and P. F. Wiley, *Chemistry of 1,2,3-Triazines and 1,2,4-Triazines, Tetrazines, and Pentazin*, John Wiley & Sons, 2009, vol. 33, pp. 1–1335.
14 A. M. Prokhorov and P. E. Progr, *Heterocycl. Chem.*, 2015, **27**, 451–464.
15 N. Saracoglu, *Tetrahedron*, 2007, **63**, 4199–4236.
16 Y. Zhou, X. Long and Y. Shu, *J. Mol. Model.*, 2010, **16**, 1021–1027.
17 J. Tu, D. Svatunek, S. Parvez, A. C. Liu, B. J. Levandowski, H. J. Eckvahl, R. T. Peterson, K. N. Houk and R. M. Franzini, *Angew. Chem., Int. Ed. Engl.*, 2019, **58**, 9043–9048.
18 C. Yongjin and B. Shuhong, *Johnson Matthey Technol. Rev.*, 2019, **63**, 51–72.
19 G. Wang, Z. Fu, H. Yin and F. Chen, *Propellants, Explos., Pyrotech.*, 2019, **44**, 1010–1014.
20 D. M. Badgujar, M. B. Talawar, S. N. Asthana and P. P. Mahulikar, *J. Hazard. Mater.*, 2008, **151**, 289–305.
21 T. M. Klapötke, *Chemistry of High-Energy Materials*, Walter de Gruyter, 2nd edn, 2012, Berlin.
22 A. E. Baydar, G. V. Boyd, P. F. Lindley and A. R. Walton, *J. Chem. Soc., Perkin Trans. 2*, 1985, **1**, 415–418.
23 Y. Wang, J. I.-C. Wu, Q. Li and P. v. R. Schleyer, *Org. Lett.*, 2010, **12**, 4824–4827.
24 P. von R. Schleyer, C. Maerker, C. A. Dransfeld, H. Jiao and N. J. R. van Eikema Hommes, *J. Am. Chem. Soc.*, 1996, **118**, 6317–6318.
25 H. Fallah-Bagher-Shaidaei, C. S. Wannere, C. Corminboeuf, R. Puchta and P. von R. Schleyer, *Org. Lett.*, 2006, **8**, 863–866.
26 Y.-F. Yang, Y. Liang, F. Liu and K. N. Houk, *J. Am. Chem. Soc.*, 2016, **138**, 1660–1667.
27 G. Sánchez-Sanz, *Tetrahedron*, 2015, **71**, 826–839.
28 J. Jusélius, D. Sundholm and J. Gauss, *J. Chem. Phys.*, 2004, **121**, 3952–3963.
29 H. Fliegl, S. Taubert, O. Lehtonen and D. Sundholm, *Phys. Chem. Chem. Phys.*, 2011, **13**, 20500–20518.
30 D. Sundholm, H. Fliegl and R. J. F. Berger, *Wiley Interdiscip. Rev. Comput. Mol. Sci*, 2016, **6**, 639–678.
31 G. Merino, T. Heine and G. Seifert, *Chem.–Eur. J.*, 2004, **10**, 4367–4371.
32 T. Heine, R. Islas and G. Merino, *J. Comput. Chem.*, 2007, **28**, 302–309.
33 R. Islas, T. Heine and G. Merino, *Acc. Chem. Res.*, 2012, **45**, 215–228.
34 M. Ernzerhof and G. E. Scuseria, *J. Chem. Phys.*, 1999, **110**, 5029–5036.
35 C. Adamo and V. Barone, *J. Chem. Phys.*, 1999, **110**, 6158–6170.
36 F. Weigend and R. Ahlrichs, *Phys. Chem. Chem. Phys.*, 2005, **7**, 3297–3305.
37 S. Grimme, J. Antony, S. Ehrlich and H. A. Krieg, *J. Chem. Phys.*, 2010, **132**, 154104.
38 N. F. Ramsey, *Phys. Rev.*, 1950, **78**, 699–703.
39 J. A. Pople, *Mol. Phys.*, 1958, **1**, 175–180.
40 R. McWeeny, *Mol. Phys.*, 1958, **1**, 311–321.
41 J. A. Gomes and R. B. Mallion, *Chem. Rev.*, 2001, **101**, 1349–1383.
42 T. Heine, C. Corminboeuf and G. Seifert, *Chem. Rev.*, 2005, **105**, 3889–3910.
43 A. Schäfer, H. Horn and R. Ahlrichs, *J. Chem. Phys.*, 1992, **97**, 2571–2577.
44 R. Ditchfield, *Mol. Phys.*, 1974, **27**, 789–807.
45 K. Wolinski, J. F. Hinton and P. Pulay, *J. Am. Chem. Soc.*, 1990, **112**, 8251–8260.
46 M. J. Frisch, G. W. Trucks, H. B. Schlegel, G. E. Scuseria, M. A. Robb, J. R. Cheeseman, G. Scalmani, V. Barone, G. A. Petersson, H. Nakatsuji, X. Li, M. Caricato, A. V. Marenich, J. Bloino, B. G. Janesko, R. Gomperts, B. Mennucci, H. P. Hratchian, J. V. Ortiz, A. F. Izmaylov, J. L. Sonnenberg, D. Williams-Young, F. Ding, F. Lipparini, F. Egidi, J. Goings, B. Peng, A. Petrone, T. Henderson, D. Ranasinghe, V. G. Zakrzewski, J. Gao, N. Rega, G. Zheng, W. Liang, M. Hada, M. Ehara, K. Toyota, R. Fukuda, J. Hasegawa, M. Ishida, T. Nakajima, Y. Honda, O. Kitao, H. Nakai, T. Vreven, K. Throssell, J. A. Montgomery, Jr., J. E. Peralta, F. Ogliaro, M. J. Bearpark, J. J. Heyd, E. N. Brothers, K. N. Kudin, V. N. Staroverov, T. A. Keith, R. Kobayashi, J. Normand, K. Raghavachari, A. P. Rendell, J. C. Burant, S. S. Iyengar, J. Tomasi, M. Cossi, J. M. Millam, M. Klene, C. Adamo, R. Cammi, J. W. Ochterski, R. L. Martin, K. Morokuma, O. Farkas, J. B. Foresman, and D. J. Fox, *Gaussian 16*, 2016.
47 GIMIC, *Version 2.0, a current density program*, 2019, can be freely downloaded from https://github.com/qmcurrents/gimic.
48 J. Ahrens, B. Geveci and C. Law, *ParaView: An End-User Tool for Large Data Visualization, Visualization Handbook*, Elsevier, 2005, see also: http://www.paraview.org.
49 M. Orozco-Ic, J. L. Cabellos and G. Merino, *Aromagnetic, a magnetic shielding program*, Cinvestav-Mérida, Mexico, 2016.
50 H. Childs, E. Brugger, B. Whitlock, J. Meredith, S. Ahern, D. Pugmire, K. Biagas, M. Miller, C. Harrison, G. H. Weber, H. Krishnan, T. Fogal, A. Sanderson, C. Garth, E. W. Bethel, D. Camp, O. Rübel, M. Durant, J. M. Favre and P. Navrátil, *Visit: An End-User Tool For*

Visualizing and Analyzing Very Large Data, 2012, see also: https://wci.llnl.gov/simulation/computer-codes/visit.
51 N. D. Charistos, A. G. Papadopoulos and M. P. Sigalas, *J. Phys. Chem. A*, 2014, **118**(6), 1113–1122.
52 E. D. Glendening, C. R. Landis and F. Weinhold, *J. Comput. Chem.*, 2013, **34**, 1429–1437.
53 J. A. Bohmann, F. Weinhold and T. C. Farrar, *J. Chem. Phys.*, 1997, **107**, 1173–1184.
54 E. Hückel, *Z. Phys.*, 1931, **70**, 204–286.
55 E. Hückel, *Z. Phys.*, 1931, **72**, 310–337.
56 P. Lazzeretti, E. Rossi and R. Zanasi, *J. Chem. Phys.*, 1982, **72**, 3129–3139.
57 R. W. A. Havenith and P. W. Fowler, *Chem. Phys. Lett.*, 2007, **449**, 347–353.
58 H. Fliegl, D. Sundholm, S. Taubert, J. Jusélius and W. Klopper, *J. Phys. Chem. A*, 2009, **113**, 8668–8676.
59 E. Steiner and P. W. Fowler, *Chem. Commun.*, 2001, **21**, 2220–2221.
60 E. Steiner and P. W. Fowler, *J. Phys. Chem. A*, 2001, **105**, 9553–9562.
61 M. Orozco-Ic, J. Barroso, N. D. Charistos, A. Muñoz-Castro and G. Merino, *Chem.–Eur. J.*, 2020, **26**, 326–330.
62 E. Steiner and P. W. Fowler, *Phys. Chem. Chem. Phys.*, 2004, **6**, 261–272.
63 G. Acke, S. Van Damme, R. W. A. Havenith and P. Bultinck, *Phys. Chem. Chem. Phys.*, 2019, **21**, 3145–3153.
64 G. Acke, S. Van Damme, R. W. A. Havenith and P. Bultinck, *J. Comput. Chem.*, 2017, **39**, 511–519.
65 J. Jusélius and D. Sundholm, *Phys. Chem. Chem. Phys.*, 1999, **1**, 3429–3435.
66 A. Stanger, *J. Org. Chem.*, 2006, **71**(3), 883–893.
67 R. Báez-Grez, L. Ruiz, R. Pino-Rios and W. Tiznado, *RSC Adv.*, 2018, **8**, 13446–13453.
68 G. Monaco and R. Zanasi, *J. Phys. Chem. A*, 2014, **118**, 1673–1683.
69 S. Pelloni, G. Monaco, P. Lazzeretti and R. Zanasi, *Phys. Chem. Chem. Phys.*, 2011, **13**, 20666–20672.